

# Path following algorithm for skid-steering mobile robot based on adaptive discontinuous posture control

Fady Ibrahim, A. A. Abouelsoud, Ahmed M. R. Fath Elbab & Tetsuya Ogata

To cite this article: Fady Ibrahim, A. A. Abouelsoud, Ahmed M. R. Fath Elbab & Tetsuya Ogata (2019): Path following algorithm for skid-steering mobile robot based on adaptive discontinuous posture control, Advanced Robotics, DOI: [10.1080/01691864.2019.1597764](https://doi.org/10.1080/01691864.2019.1597764)

To link to this article: <https://doi.org/10.1080/01691864.2019.1597764>



[View supplementary material](#)



Published online: 02 Apr 2019.



[Submit your article to this journal](#)



CrossMark

[View Crossmark data](#)



## Path following algorithm for skid-steering mobile robot based on adaptive discontinuous posture control

Fady Ibrahim<sup>a,b</sup>, A. A. Abouelsoud<sup>c</sup>, Ahmed M. R. Fath Elbab<sup>a,d</sup> and Tetsuya Ogata<sup>b</sup>

<sup>a</sup>Mechatronics and Robotics Engineering Department, Egypt-Japan University of Science and Technology (E-JUST), Borg Elarab, Alexandria, Egypt; <sup>b</sup>Department of Intermedia Art and Science, Waseda University, Tokyo, Japan; <sup>c</sup>Electronics and Communications Engineering Department, Cairo University, Giza, Egypt; <sup>d</sup>On leave from Mechanical Engineering Department, Assiut University, Assiut, Egypt

### ABSTRACT

The kinematic model of a skid-steering mobile robot (SSMR) is manipulated using signed polar transformation which represents a discontinuous state transformation. The influence of relative position between the instantaneous center of rotation (ICR) and SSMR center of mass is considered. Then, adaptive state feedback controller is designed and stability regions are studied. Subsequently, a point-to-point tracking algorithm is introduced to track a trajectory that is defined by a set of way-points, which is the more realistic case of dangerous exploration or landmine detection purposes. The closed-loop system is simulated using MATLAB environment and experimentally validated using a modified TURTLEBOT3 Burger. Results show that the proposed controller reaches almost zero steady state error with smooth paths for point stabilization, moreover, good tracking capabilities are demonstrated. The proposed control system integrates both posture and tracking algorithm, thus achieve trajectory tacking which is defined by a set of way-points.

### ARTICLE HISTORY

Received 21 March 2018  
Revised 15 November 2018  
and 21 February 2019  
Accepted 28 February 2019

### KEYWORDS

SSMR; signed polar coordinates; adaptive control; discontinuous control; point-to-point tracking

## 1. Introduction

SSMR is popular to provide superior traction capabilities further mechanical robustness; by virtue of the all-wheel propulsion and limited degree of freedom for the wheels as they does not have a separate steering system [1]. Thus, SSMR is commonly used for navigation purposes across unprepared terrains such as landmine detection, hazard rescue and dangerous exploration. Different wheel speeds cause steering of SSMR, thus lateral velocity occurs associated with side skidding. Although this system is open-loop controllable, it has been proved that this system is non-stabilizable using smooth time-invariant state feedback [2]. However, it is clear that the kinematic model of SSMR is driftless, underactuated, highly coupled, nonlinear system associated with nonholonomic constraints. Thus, the design of a posture stabilizing controller for this system is a challenging topic in control engineering.

It is an interesting fact that solving the problem of predefined trajectory tracking is easier than point stabilization for nonholonomic (WMR) where linear state feedback could stabilize WMR about a predefined trajectory [3]. Thus, it is noticed that, tracking a predefined trajectory which is representable by equation(s) is mostly

addressed in the literature. Additionally, path planning control in real applications of WMR will not generate circular, sinusoidal, quadratic, or even infinity-like trajectories. Also, thinking about dynamic obstacle avoidance, then it is not realistic to design a model-based control law to track predefined trajectory.

### 1.1. Related work

The control of WMR concerns about designing of control law to vanish the error state vector for either posture stabilization or trajectory tracking. Based on Brockett [2], several controllers have been proposed for point stabilization [4–11]. These controllers are classified as nonlinear control methods [4–6], discontinuous controllers [7–9] and time-varying state feedback [10, 11].

Nonlinear point stabilization controllers for the unicycle-like mobile robot are addressed in [4–6] using Lyapunov stability method. Skidding and wheel floating are analyzed using the kinematic model in [4]. System dynamics are considered in simulations and compared to experiments, where asymptotic stability is achieved with none smooth paths. Additionally, bijective kinematic model is used in [5] by introducing a modified

**CONTACT** Fady Ibrahim fady.ibrahim@ejust.edu.eg Mechatronics and Robotics Engineering Department, Egypt-Japan University of Science and Technology (E-JUST), PO Box 21934, Borg Elarab, Alexandria, Egypt

On leave from Research Fellow, Department of Intermedia Art and Science, Waseda University, Tokyo, Japan.

Supplemental data for this article can be accessed here. <https://doi.org/10.1080/01691864.2019.1597764>

© 2019 Informa UK Limited, trading as Taylor & Francis Group and The Robotics Society of Japan

four states model, moreover, polar state transformation is used in [6] for both point stabilization and path tracking. Circular and linear trajectories are used to show the effectiveness of the proposed controller, while path following controller is singular around the origin.

Discontinuous controllers are addressed in [7–9] to regulate the unicycle-like mobile robot. Backstepping technique is used in [7] and stability is proved by Lyapunov second method, subsequently, adaptive terms are introduced to overcome the input disturbance. The effectiveness of this method is illustrated by simulation. Furthermore, an extended Lyapunov function is presented in [8] based on the kinematic model. The proposed controller can steer the system to the desired point, however, it suffers from fore-and-aft motion. A polar state representation is used in [9] for controller design to achieve point regulation with a smooth path and without direction inversion.

Time-varying controllers based on the kinematic model are introduced in [10, 11]. A Mamdani FIS is proposed in [10] to adapt the parameters of a Lyapunov control function. Asymptotic stability of SSMR with smooth paths is showed by means of numerical simulation. A global  $K$ -exponential output feedback signals are introduced in [11]. The model is transformed to chained form and studied using time-varying coordinate transformation. It is clear that the model of unicycle-like mobile robot departs from that of SSMR, because the none-zero value of  $X_{ICR}$  causes state coupling in SSMR.

On the other hand, trajectory tracking controllers are addressed in many researches [12–44], and may be classified to predefined trajectory [12–38] and a point-to-point trajectory [39–44]. The model of WMR is simplified to a point with two-degree of freedom in [12, 13]. A time-varying state feedback controller using backstepping is introduced in [12] and numerical simulation is used to demonstrate the effectiveness of this method. Furthermore, the inverse kinematics of the WMR is used in [13] for controller design, while TS-FIS is used to generate the control gains. This approach is proved to be stable by Lyapunov second method and validated experimentally.

Steering controllers are addressed in [14, 15] using constant longitudinal speed to achieve trajectory tracking. Steering control of WMR is addressed in [14], using small angle approximation to simplify the model non-linearity, subsequently, a proportional constant gain is used to regulate the desired angle error. Additionally, the actuator limitations are considered in [15] by a standard saturation function and regulation algorithm for longitudinal speed at corners, while proper tracking is shown by simulation.

Sliding mode control (SMC) and super-twisting algorithms (STA) are used for WMR tracking as in [16–19].

A robust SMC is addressed in [16], and stability is proved by Lyapunov direct method. The effectiveness of this controller is illustrated by simulations of circular paths. State feedback controller based on STA is proposed in [17] for SSMR. Both simulation and experiments are compared with state feedback and first order SMC. Super-twisting sliding mode control is addressed in [18] for WMR, which imposes a second order sliding mode followed by PD control to eliminate chattering and compensate for dynamics. Experiments demonstrate the effectiveness of this controller. Furthermore, an adaptive STA for SSMR is proposed in [19], thus gains are adjusted regularly to keep the control effort as minimal as possible. This method is validated experimentally on a circular path tracking.

Intelligent methods as neural networks (NN), heuristic optimization techniques and model predictive control (MPC) are proposed in [20–26] for path following control of WMR to overcome parameters uncertainties, external disturbances and actuator limitations. A MPC is presented in [20] and extended for obstacle avoidance. Three heuristic optimization techniques are evaluated and PSO is selected for real implementation. A MPC with online model learning is introduced in [21] to generate an optimal policy based on the learned SSMR model, where tires and road conditions are considered with experimental validation. A MPC is proposed in [22] where quadratic cost function includes tracking error and control effort which is minimized by the proposed controller. Tracking capabilities are demonstrated by simulation and real robot validation. A compound sine function NN and an improved compound cosine function NN are introduced in [23, 24] with simple structure and continuous learning algorithm. These methods are simulated for circular and sinusoidal trajectories. Reinforcement learning-based adaptive neural tracking algorithm is proposed in [25], where skidding and slipping are addressed and tested by simulations. An adaptive type-2 Takagi-Sugeno fuzzy-neural PID controller is introduced in [26] with online learning algorithm to update the control parameters, thus compensate for disturbance. This controller is tested in a line tracking.

Adaptive control techniques are shown in [27–30] for predefined trajectory tracking of unicycle-like mobile robot. An adaptive control law is designed in [27] beside two observers to estimate system inputs, subsequently a circle tracking simulation is presented. Lyapunov function controllers are introduced in [28–30] with gain scheduling, where longitudinal slip is considered in simulations, while external disturbances and parameters uncertainty are considered in [30].

Robust controllers are integrated with observers as in [31–38] for predefined trajectory tracking, to estimate unmeasurable parameters and disturbances.

Backstepping controller is integrated with UKF in [31] to estimate longitudinal and lateral slipping, however, the model of SSMR is simplified to unicycle-like mobile robot. A robust  $H_\infty$  state feedback control with mixed GA and LMI are proposed in [32] for car-like model without lateral velocity sensation. PD iterative learning control for omni-directional mobile robot is presented in [33], additionally square trajectory tracking is illustrated by both simulation and experiments. An extended state observer is used in [34] to overcome the state disturbances, this approach is simulated on a line and circle tracks. Robustness analysis is carried out in [35] using numerical simulation to ensure bounded state; provided that WMR moves slowly and with small uncertainties. A robust finite-time control with velocities observers is proposed in [36] and is validated by numerical simulations. A robust controller is proposed in [37] by integrating adaptive fuzzy variable structure kinematic controller, and PD dynamic controller. Simulations and experimental validation show the effectiveness of this approach. Disturbance observer and adaptive compensator are designed in [38], where simulations of circular trajectories are presented.

The other approach is the point-to-point trajectory tracking [39–44], where the desired trajectory is represented by a set of way-points or arcs and lines. A robust sliding mode fuzzy logic control for SSMR is addressed in [39], where continuous reference trajectory is generated using quadratic curve fitting, furthermore the proposed FIS is validated experimentally. Set of sectors are defined in [40] using the way-points to calculate the desired orientation of SSMR. The control between points is achieved by PID controller, subsequently physical validation is conducted in line, step, and three way-points trajectories. Arc fitting is proposed in [41], where circular arcs are generated to calculate the desired radius of curvature based on simplified model of SSMR. FIS is used to track piece-wise linear paths in [42], where the smooth reference path is approximated by piece-wise lines, afterwards simulations demonstrate the feasibility of this FIS. Linear PD controller driven by tracking error is presented in [43], and [44] proposed a smooth feedback control law, where reference path is identified as a set of lines or circular arcs.

## 1.2. Motivation and paper contribution

The main contribution of this paper is the design of a discontinuous controller using the signed polar state transformation. This controller is applied to the under-actuated, nonlinear, driftless kinematic model of SSMR considering the effect of ICR location. The proposed controller is designed to achieve smooth paths without

fore-and-aft motion, additionally adaptive gain calculation algorithm is introduced to ensure the controller applicability using any actuators. Subsequently, a point-to-point tracking algorithm is proposed based on the knowledge of next point on the trajectory which is more realistic case in dynamic obstacle avoidance and unstructured environment navigation.

We emphasize that the predefined trajectory tracking, where trajectory is defined via equation(s) is impractical in real application of autonomous WMR especially in unprepared terrain. Also, it is well known that path planning controller more likely generates the desired path in form of certain way-points. Based on that, our approach is to integrate the adaptive discontinuous control with tracking algorithm to achieve the point-to-point path tracking.

*Paper Construction:* This paper consists of five sections besides the introduction and is organized as follows: Section 2 presents the kinematic model of SSMR. Signed polar coordinate transformation is proposed in Section 3. Then Section 4 point-to-point tracking algorithm is proposed and controller design with stability analysis. After that Section 5 is for results and discussion. Finally, conclusions are drawn in Section 6.

## 2. Kinematic model of SSMR

To analyze the kinematics of SSMR, a local coordinate frame is considered at the center of gravity (COG) of SSMR denoted by  $(x, y, z)$ . SSMR is studied while moving in a horizontal plane formed by  $X_w$  and  $Y_w$  of the world frame ( $X_w, Y_w, Z_w$ ) as illustrated in Figure 1. Suppose that SSMR has linear velocity vector  $v = [v_x \ v_y \ 0]^T$  and angular velocity vector  $\omega = [0 \ 0 \ \omega_z]^T$ , see Figure 1. The state vector  $q$  of SSMR with respect to the world frame is  $q = [X \ Y \ \theta]^T$ , where  $X$  and  $Y$  represent the coordinates of COG in the world frame and  $\theta$  represents the angle between  $x$ -axis of the local coordinate frame and the  $X_w$ -axis of the world frame. Hence the generalized velocity vector  $\dot{q}$  is governed by Equation (1), where  $\dot{q} = [\dot{X} \ \dot{Y} \ \dot{\theta}]^T$ .

$$\dot{q} = \begin{bmatrix} \cos \theta & -\sin \theta & 0 \\ \sin \theta & \cos \theta & 0 \\ 0 & 0 & 1 \end{bmatrix} \begin{bmatrix} v_x \\ v_y \\ \omega_z \end{bmatrix}. \quad (1)$$

The driving mechanism of the SSMR depends on two motors, one for each side of the SSMR. The tires on the same side have the same angular speed. The steering of SSMR depends on variation of linear speed for each side, thus lateral slip occurs and causes the SSMR to rotate about  $z$ -axis to steer. Based on that all the tires are not tangent to the path of SSMR during turning. Assuming that SSMR has angular velocity  $\omega_z$  about an Instantaneous Center of Rotation (ICR), and the ICR has has

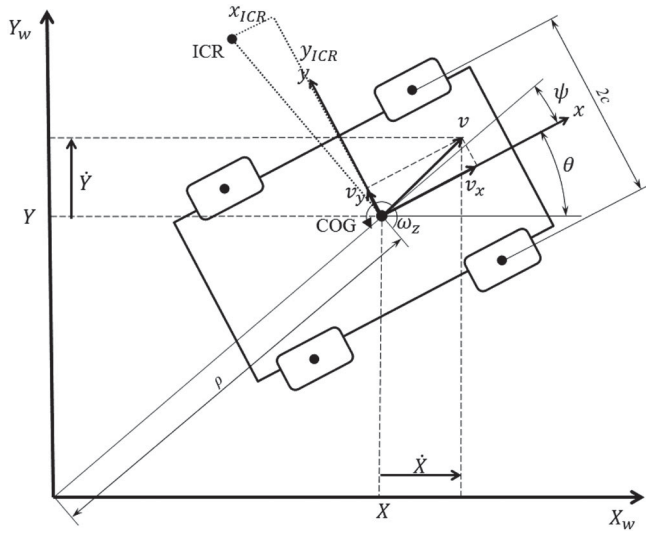


**Figure 1.** Velocities of SSMR with respect to world coordinate frame and local coordinate frame.

coordinates  $x_{ICR}$  and  $y_{ICR}$  with respect to the local coordinate frame  $(x, y, z)$  as illustrated in Figure 1. The lateral velocity  $v_y$  depends on  $\omega_z$  and  $x_{ICR}$  which represents the nonholonomic constraint, subsequently (2) is derived from (1) [45].

$$\dot{q} = \begin{bmatrix} \cos \theta & x_{ICR} \sin \theta \\ \sin \theta & -x_{ICR} \cos \theta \\ 0 & 1 \end{bmatrix} \begin{bmatrix} v_x \\ \omega_z \end{bmatrix}. \quad (2)$$

It worth to mention that the value of  $x_{ICR}$  is significant in SSMR behavior, moreover SSMR will be uncontrollable if ICR became outside SSMR dimensions in longitudinal direction, additionally ICR is not coincident with the lateral axis  $y$  during turns [46]. The existence of none zero  $x_{ICR}$  in Equation (2) causes coupling between states, yielding dependency of states. Also none zero  $x_{ICR}$  prevents the regulation of one state away from other states. It is clear that (2) is underactuated, driftless system, thus we proposed a discontinuous state transformation as illustrated in Section 3.

### 3. Signed polar coordinates state transformation

To analyze system (2), a signed polar state transformation is introduced. The state vector  $q$  is transformed to signed polar state vector  $p$  where  $p = [\rho \psi \theta]^T$  as illustrated in Figure 1. The state  $\rho$  is the distance between the COG and the origin of the world frame, while the state  $\psi$  is the angle between the  $x$ -axis and the line represented by  $\rho$ . It should be mentioned that the value of  $\rho$  is positive in the right half plane and negative in the left half of the world

plane. Where

$$\rho = \text{sgn}(X)\sqrt{X^2 + Y^2}, \quad (3)$$

$$\psi = \tan^{-1}\left(\frac{\text{sgn}(X)Y}{|X|}\right) - \theta. \quad (4)$$

This leads to

$$X = \rho \cos(\psi + \theta), \\ Y = \rho \sin(\psi + \theta). \quad (5)$$

Equations (6–8) represent the first derivative of the polar state vector  $p$  with respect to time where  $X \neq 0$ .

$$\dot{\rho} = \frac{X\dot{X} + Y\dot{Y}}{\rho}, \quad (6)$$

$$\dot{\psi} = \frac{X\dot{Y} - Y\dot{X}}{\rho^2} - \dot{\theta}, \quad (7)$$

$$\dot{\theta} = \omega_z. \quad (8)$$

Substituting +++(2, 5) in (6–8) will lead to equation (9) which is the kinematic model of SSMR represented in signed polar coordinates.

$$\dot{p} = \begin{bmatrix} \cos \psi & -x_{ICR} \sin \psi \\ -\sin \psi & \frac{x_{ICR} \cos \psi}{\rho} - 1 \\ 0 & 1 \end{bmatrix} \begin{bmatrix} v_x \\ \omega_z \end{bmatrix}. \quad (9)$$

It is clear from Equation (9) that the mentioned signed polar state transformation introduces discontinuity at  $\rho = 0$ . Although (2) is smooth, system (9) has a discontinuity at the origin. This discontinuity is essential to design the regulation control law, this is consistent with Brockett [2].

### 4. Path following controller design

Most of the previous researches study the tracking problem of WMR based on an assumption that the desired trajectory is well known and defined by equation(s). But in the real cases which include unstructured environment navigation or dynamic obstacle avoidance, the desired path may be defined as a set of state points that the mobile robot has to pass through them in sequence.

#### 4.1. Path following algorithm

In this section, we propose a Path Following algorithm and a discontinuous posture control law which is proposed in Section 4.2, thus get benefits of both methods. The proposed path following algorithm requires only the current state of the SSMR and the next point on

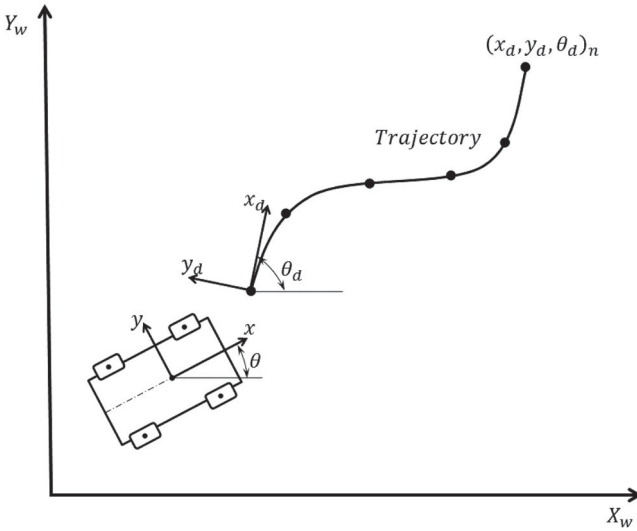


**Figure 2.** Trajectory tracking concept.

the trajectory. In addition, it is remarkable that the proposed method uses a variable control commands rather than other tracking algorithms which consider constant longitudinal speed.

#### Algorithm 1 (Path Following).

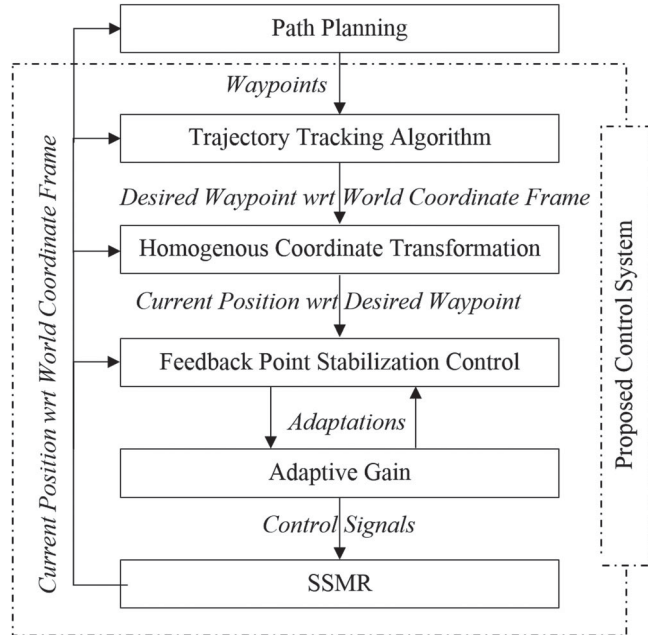
- (1) Get the current state  $[X \ Y \ \theta]^T$  of SSMR in world coordinate frame
- (2) Find the target point  $q_{\text{target}} = [X_d \ Y_d \ \theta_d]^T$  on the desired trajectory with respect to the world coordinate frame
- (3) Transform the current position of SSMR with respect to goal point using homogeneous transformation as illustrated in Equation (10)  $[\tilde{X} \ \tilde{Y} \ \tilde{\theta}]^T$
- (4) Apply the control law ((16), (17))
- (5) When the magnitude of the error vector  $(\sqrt{\tilde{X}^2 + \tilde{Y}^2 + \tilde{\theta}^2})$  becomes less than the tracking tolerance ( $\epsilon$ ), go to step 1

Figure 2 illustrates the main concept of this algorithm. Also, the overall structure of the control system is illustrated in Figure 3 where all subsystems are integrated to achieve tracking.

$$\begin{bmatrix} \tilde{X} \\ \tilde{Y} \\ \tilde{\theta} \end{bmatrix} = \begin{bmatrix} \cos \theta_d & \sin \theta_d & 0 \\ -\sin \theta_d & \cos \theta_d & 0 \\ 0 & 0 & 1 \end{bmatrix} \begin{bmatrix} X - X_d \\ Y - Y_d \\ \theta - \theta_d \end{bmatrix}. \quad (10)$$

#### 4.2. Posture controller design

In this section, we propose a discontinuous state feedback control law to regulate the position and orientation of SSMR about an arbitrary desired point.



**Figure 3.** The proposed control system structure.

It is well known that the system (2) should be treated either with nonlinear or time-varying or discontinuous control according to Brockett's condition [2].

There are three reasons to use the discontinuous control in this work over time-varying and nonlinear controls. Firstly, time-varying control mainly exhibits oscillatory paths and suffers from slow convergence near the equilibrium point [11, 47–50], and this is due to the periodic functions that are used in time-varying techniques. Secondly, nonlinear methods [31, 51–56] are applied to dynamic models with kinematic constraints which are not driftless and not the current case of study. Finally, discontinuous control shows better convergence rate near the origin due to the discontinuity at the origin [57–59]. Also, the proposed controller is designed to achieve smooth paths to overcome the drawback of fore-and-aft motion [8, 60, 61]. We use the signed polar coordinates to represent system (2) in the form (9) which has a discontinuity at the origin as mentioned in Section 3.

System (9) is manipulated by a control transformation (12) to be in the form of (11).

$$\dot{p} = \begin{bmatrix} 1 & 0 \\ \frac{\sin \psi}{x_{\text{ICR}}} & 1 + \frac{\rho \cos \psi}{x_{\text{ICR}}} \\ \frac{\sin \psi}{x_{\text{ICR}}} & -\frac{\rho \cos \psi}{x_{\text{ICR}}} \end{bmatrix} \begin{bmatrix} v_1 \\ v_2 \end{bmatrix}, \quad (11)$$

where  $v_1$  and  $v_2$  are new controls governed by the invertible transformation (12), ( $x_{\text{ICR}} \neq 0$ )

$$\begin{bmatrix} v_1 \\ v_2 \end{bmatrix} = \begin{bmatrix} \cos \psi & -x_{\text{ICR}} \sin \psi \\ -\sin \psi & -\frac{x_{\text{ICR}} \cos \psi}{\rho} \end{bmatrix} \begin{bmatrix} v_x \\ \omega_z \end{bmatrix}. \quad (12)$$

Equation (11) is rewritten as following.

$$\begin{bmatrix} \dot{\rho} \\ \dot{\psi} + \dot{\theta} \end{bmatrix} = I_2 \begin{bmatrix} v_1 \\ v_2 \end{bmatrix}, \quad (13)$$

where  $I_2$  is an identity matrix of size 2.

Choosing the controls  $v_1$  and  $v_2$  such that  $k_1$  and  $k_2$  are positive constants

$$v_1 = -k_1 \rho, \quad (14)$$

$$v_2 = -k_2(\psi + \theta). \quad (15)$$

Substituting Equations (14, 15) in (12), the control law  $v_x$  and  $\omega_z$  are as following.

$$v_x = \rho(k_2(\psi + \theta) \sin \psi - k_1 \cos \psi), \quad (16)$$

$$\omega_z = \frac{\rho}{X_{\text{ICR}}} (k_2(\psi + \theta) \cos \psi + k_1 \sin \psi). \quad (17)$$

We emphasize that control signals (16), (17) are bounded for all values of  $\rho, \psi$  and  $\theta$ , regardless the discontinuity at the origin in Equation (9).

### 4.3. Stability analysis

Substituting Equation (14) in (13) leads to  $\dot{\rho} = -k_1 \rho$  which will guarantee exponential asymptotic stability of  $\rho$ . Similarly using Equation (15) in (13) will guarantee the exponential convergence to zero of the summation  $(\psi + \theta)$ .

It is clear that the summation  $(\psi + \theta)$  will converge to zero in one of the following cases:

- case 1;  $\psi = 0$  and  $\theta = 0$

In this case, the asymptotic stability is achieved.

- case 2;  $\psi = -\theta \neq 0$

This means that,  $\theta$  and  $\psi$  have the same absolute value with different sign. It is clear from Figure 1 that this case occurs only if  $Y = 0$ , also substituting the condition  $\psi = -\theta$  in Equation (4) leads to  $\tan^{-1}(Y/X) = 0$  which also means that  $Y = 0$ .

Further analysis shall be conducted in this case to analyze instability conditions, substituting the condition  $\psi = -\theta \neq 0$  in ((16), (17)) the control signals  $v_x, \omega_z$  became as in ((18), (19)).

$$v_x = -k_1 \rho \cos \psi, \quad (18)$$

$$\omega_z = \frac{k_1 \rho \sin \psi}{X_{\text{ICR}}}. \quad (19)$$

Four sub-cases will be considered:

*Case 2.1 ( $\rho \neq 0$  and  $\psi \neq \pm n\pi/2$ ,  $n$  is an integer)*

This means that Equations ((18), (19)) will not equal to zero and SSMR will have longitudinal and rotational speeds.

*Case 2.2 ( $\rho \neq 0$  and  $\psi = \pm n\pi/2$ ,  $n$  is an odd integer.)*

In this case, Equation (18) will tend to zero while the control signal  $\omega_z$  represented by Equation (19) will have none-zero value. Thus SSMR will rotate about  $z_{\text{axis}}$  and the *ICR* effect (1) will change SSMR position.

*Case 2.3 ( $\rho \neq 0$  and  $\psi = \pm n\pi$ ,  $n$  is an integer.)*

In this case, the mobile robot will not rotate about  $z_{\text{axis}}$  as Equation (19) will vanish, and it will move along  $x_{\text{axis}}$  with the same orientation.

*Case 2.4 ( $\rho = 0$ )*

This means that SSMR reaches the origin with incorrect orientation.

From the above discussion, it is clear that in cases (2.1–2.2) the condition  $\psi = -\theta \neq 0$  is a temporary condition and will vanish as long as there is at least one control signal is not equal to zero, thus the closed-loop system will converge.

While Case (2.3) the control law (17) will not correct the orientation of SSMR. Additionally, Case (2.4) means that SSMR reaches the desired point with incorrect orientation, this could be avoided by proper selection of the control gains  $k_1$  and  $k_2$  through rapid orientation correction.

From the above analysis, we can conclude that the control law ((16), (17)) will guarantee the asymptotic stability of SSMR except when the initial condition  $q_i$  is equal to ( $q_i = [0 \ 0 \ \theta]^T$ ) or ( $q_i = [X_i \ 0 \ \pm \pi]^T$ ). It worth to mention that this control law is proposed to be used in a tracking algorithm, and it is clear that the two exceptions that mentioned above are not likely to happen in a smooth trajectory tracking as will be illustrated in Section 4.

### 4.4. Adaptation of control signals

In order to put the control signals ((16), (17)) in the order of magnitude which is suitable for the actuators of any mobile robot. It is required to adapt the control gains  $k_1$  and  $k_2$  such that the motors can achieve the control signals. We propose an adaptive proportional saturation algorithm, which ensures the applicability of the control signals. It is important to mention that this algorithm will not influence the effect of the original control law but only adapt the control gains  $k_1$  and  $k_2$ . We consider the maximum capability of any motor by the maximum longitudinal speed that the mobile robot can achieve  $v_{\max}$ . The wheels of SSMR have longitudinal speeds governed by Equation (20).

$$\begin{bmatrix} v_L \\ v_R \end{bmatrix} = \begin{bmatrix} 1 & -c \\ 1 & c \end{bmatrix} \begin{bmatrix} v_x \\ \omega_z \end{bmatrix}, \quad (20)$$

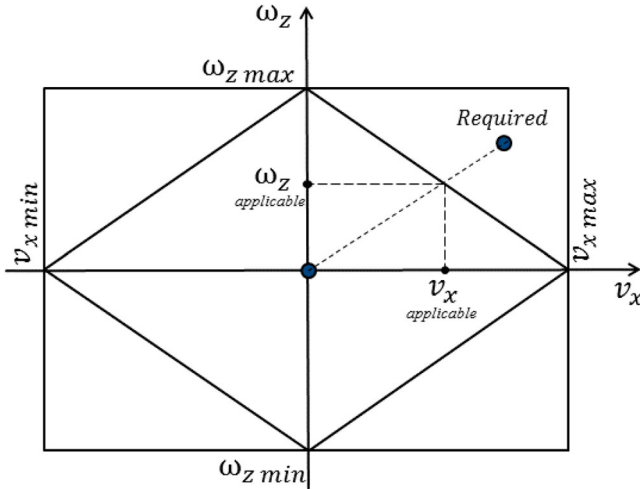


**Figure 4.** The principle of actuator capacity proportional saturation.

where  $c$  is half the distance between left and right tires as illustrated in Figure 1,  $v_L$  and  $v_R$  are left and right wheels longitudinal velocities respectively.

#### Algorithm 2 (Adaptive Proportional Saturation).

- (1) Calculate the required maximum absolute longitudinal speed  $v_{\text{req}}$  for each side of wheels.  $v_{\text{req}} = \max a(|v_L|, |v_R|)$
- (2) Calculate the correction factor  $\zeta$ , where  $\zeta = v_{\text{max}}/v_{\text{req}}$
- (3) If  $\zeta < 1$  then:  $k_1^{\text{ad}} = k_1\zeta$  and  $k_2^{\text{ad}} = k_2\zeta$  then recalculate  $v_x$  and  $\omega_z$  using  $k_1^{\text{ad}}$  and  $k_2^{\text{ad}}$

Where  $k_1^{\text{ad}}$  and  $k_2^{\text{ad}}$  are the adapted control gains.

Based on that all the control signals are proportionally adapted to be within the actuator capacity, this will guarantee that the proposed controller is applicable to any real platform.

Figure 4 illustrates the principle of actuator capacity adaptive proportional regulation. The outer rectangle represents the maximum capacity of the actuator such that the SSMR will move in a straight line or even rotate without translation. But in case that SSMR is required to perform a general plane motion; the inner rhombus represents the actual capacity of the motors. Thus, if the required control command is outside the capacity rhombus the described Algorithm 2 should be applied.

## 5. Results and analysis

In this section the simulation environment is mentioned and physical mobile robot which is used in validation

**Table 1.** Simulation parameters.

| Parameter        | Value      |
|------------------|------------|
| $x_{\text{ICR}}$ | 0.045 (m)  |
| $k_1$            | 1.2        |
| $k_2$            | 1.5        |
| $c$              | 0.1435 (m) |
| $v_{\text{max}}$ | 0.2 (m/s)  |

described. The localization system of the SSMR is described, and the ROS nodes map is demonstrated. After that both simulation and physical validation results are presented for the posture controller followed by the results of the path tracking controller.

### 5.1. Test environment

The proposed control system is simulated in MATLAB environment using parameters that are tabulated in Table 1. It is worth to mention that, in real motion  $x_{\text{ICR}}$  depends on many parameters based on the robot dynamics, some previous researches designed an observer to estimate the location of ICR. We do not estimate the location of the ICR, but we consider  $x_{\text{ICR}}$  is a constant with a relatively large value relative to the size of the SSMR, then we designed a controller that could regulate the SSMR motion. As mentioned in the modeling Section 2; the term  $x_{\text{ICR}}$  causes coupling between states and prevents the regulation of one state away from other states. This means that higher the value of  $x_{\text{ICR}}$ , the higher the state coupling. By considering high value of  $x_{\text{ICR}}$  (our assumption), we designed a controller which could regulate a highly coupled system, which is much more complicated task. During physical experiments, the ICR location varies depending on the path curvature, however it is remarkable that the proposed controller which uses

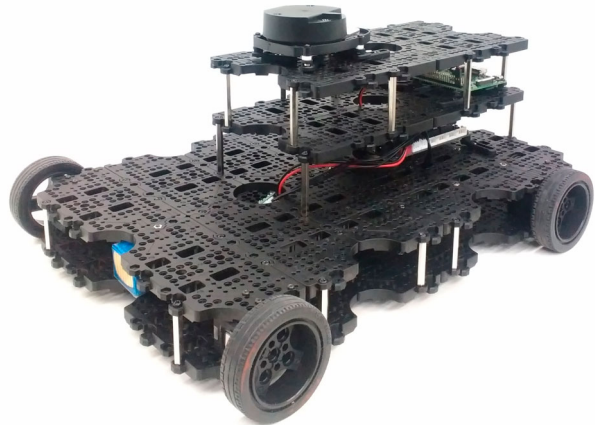


**Figure 5.** A reconfigured TURTLEBOT3 Burger (SSMR).

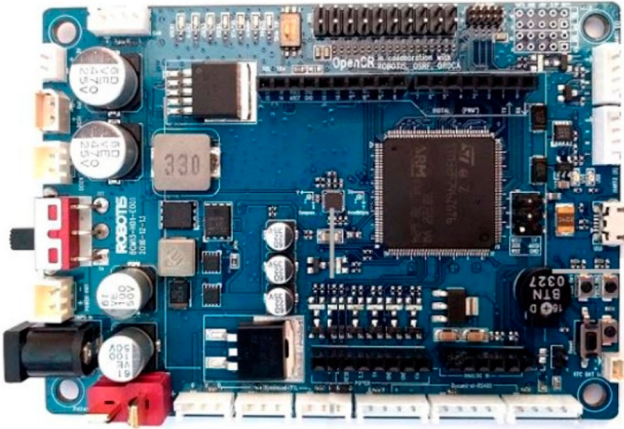


**Figure 6.** OpenCR 1.0, A low-level control board integrated with 9-axis IMU.

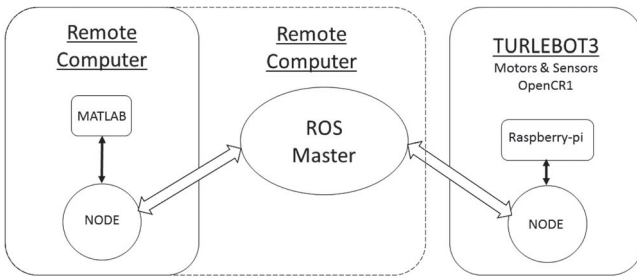


**Figure 7.** The main concept of ROS nodes connections.

a relatively large fixed  $x_{ICR}$  succeeded to vanish the error state as presented in this section.

Subsequently, experiments are carried out using a modified TURTLEBOT3 Burger shown in Figure 5. The TURTLEBOT3 Burger [62] is reconfigured to be SSMR. Based on actuators capacity and SSMR dimensions,

the maximum longitudinal speed is 0.2 m/s while the maximum rotational speed is 1.3938 rad/s. The mobile robot is actuated by 4 servo motors attached to 33 mm radius tires, low-level control board shown in Figure 6 (OpenCR1) [63] which is equipped with 9-axis IMU as well, and a SBC Raspberry-pi3. The mobile robot is controlled by a remote-PC over Wi-Fi network in ROS environment. ROS and Raspberry-pi are used to receive data from the robot and send commands to the robot, while all calculations are performed in the remote-PC. Figure 7 demonstrates the connection of different items of the experimental work.

The mobile robot is localized using odometry, the traveled distance is measured by 4096 PPR contact-less absolute encoder 12Bit [64] which is attached to the wheels, while the angle of rotation is measured by the IMU which is integrated with the OpenCR1.0 board shown in Figure 6. It is well known that odometry can estimate the location of the mobile robot with accumulated error, the total localization error is found to be less than 2% in the described robot on a solid smooth slab. On the other hand, the accuracy of the localization system will not affect the judgment of the control law. The control signal is a function of the robot state vector and is used to regulate the robot state vector. In other words, the control law is proved to achieve the goal within the accuracy of the localization system.

## 5.2. Posture controller results

Five different cases are tested using the proposed controller, while the desired destination i.e.  $q_{\text{target}}$  is the origin with an orientation parallel to  $X_w$ -axis, i.e.  $q_{\text{target}} = [0 \ 0 \ 0]^T$ . The initial conditions and the steady state errors

**Table 2.** Initial conditions and steady state error for point stabilization.

|                           | Case                      | 1                     | 2                     | 3                     | 4                     | 5                     |
|---------------------------|---------------------------|-----------------------|-----------------------|-----------------------|-----------------------|-----------------------|
| Initial Conditions        | $X_i(\text{m})$           | 3                     | -2.5                  | 1                     | 2                     | -1                    |
|                           | $Y_i(\text{m})$           | 2                     | 1.5                   | 0                     | 1                     | -2                    |
|                           | $\theta_i(\text{rad})$    | 1                     | -1                    | $\pi/2$               | 0                     | $\pi$                 |
| steady State Error (Sim.) | $X_{ss}(\text{m})$        | $3.1 \times 10^{-5}$  | $2.6 \times 10^{-4}$  | $9.9 \times 10^{-4}$  | $6.3 \times 10^{-4}$  | $-4.9 \times 10^{-4}$ |
|                           | $Y_{ss}(\text{m})$        | $-6.6 \times 10^{-4}$ | $3.8 \times 10^{-5}$  | $-1.5 \times 10^{-5}$ | $4.7 \times 10^{-5}$  | $-1.1 \times 10^{-4}$ |
|                           | $\theta_{ss}(\text{rad})$ | $6.6 \times 10^{-4}$  | $-9.6 \times 10^{-4}$ | $6.9 \times 10^{-4}$  | $-9.8 \times 10^{-4}$ | $-9.9 \times 10^{-4}$ |
| Steady State Error (Exp.) | $X_{ss}(\text{m})$        | 0.0093                | -0.0093               | 0.0088                | 0.0055                | -0.0076               |
|                           | $Y_{ss}(\text{m})$        | -0.0014               | -0.0031               | 0.0020                | -0.0038               | 0.0032                |
|                           | $\theta_{ss}(\text{rad})$ | 0.0017                | $-5.6 \times 10^{-4}$ | $-8.9 \times 10^{-4}$ | 0.0035                | 0.0030                |

**Table 3.** The values of  $\Sigma$ ,  $\tau$  and  $Drift_{\max}$  for the four cases.

|                          | Case                       | 1                    | 2                    | 3      | 4      | 5      |
|--------------------------|----------------------------|----------------------|----------------------|--------|--------|--------|
| Initial State Simulation | $\Sigma_i$                 | 3.7417               | 3.0822               | 1.8621 | 2.2361 | 3.8516 |
|                          | $\Sigma_{ss}^{\text{sim}}$ | $9.3 \times 10^{-4}$ | $9.9 \times 10^{-4}$ | 0.0012 | 0.0012 | 0.0011 |
| Experimental             | $\tau^{\text{sim}}(s)$     | 21.560               | 18.010               | 7.780  | 15.100 | 19.240 |
|                          | $\Sigma_{ss}^{\text{exp}}$ | 0.0096               | 0.0098               | 0.0091 | 0.0075 | 0.0088 |
|                          | $\tau^{\text{exp}}(s)$     | 21.871               | 18.319               | 8.234  | 15.673 | 19.91  |
|                          | $Drift_{\max}(\text{m})$   | 0.0347               | 0.0248               | 0.0039 | 0.0177 | 0.0584 |

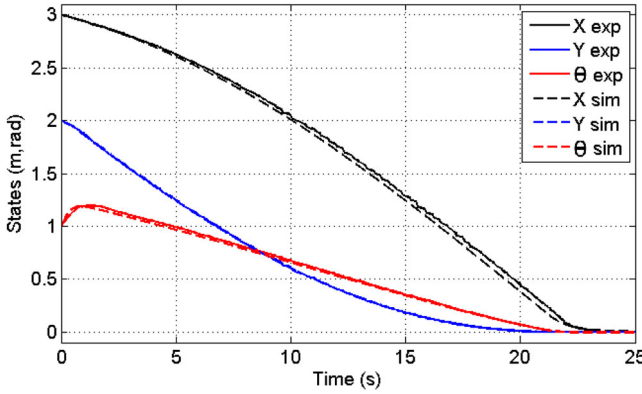


**Figure 8.** Time response of states  $X(m)$ ,  $Y(m)$ ,  $\theta(\text{rad})$  of SSMR Case (1).

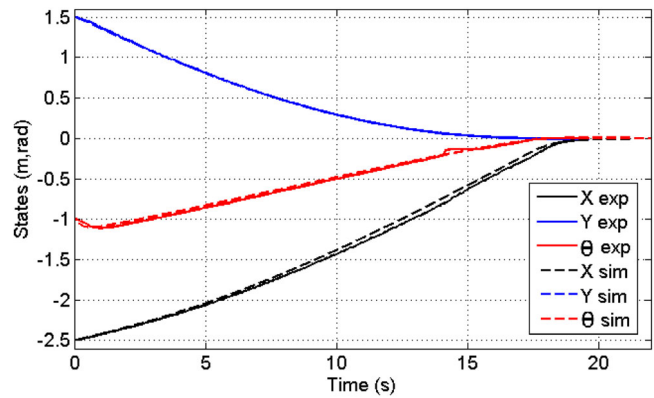


**Figure 10.** Time response of states  $X(m)$ ,  $Y(m)$ ,  $\theta(\text{rad})$  of SSMR Case (2).

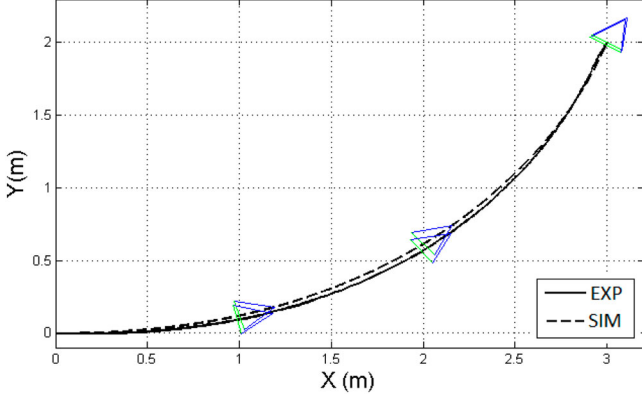


**Figure 9.** The  $X$ - $Y$  diagram for Case (1).

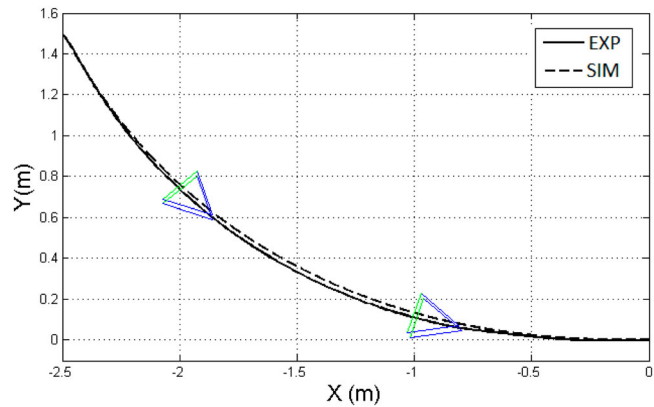


**Figure 11.** The  $X$ - $Y$  diagram for Case(2).

are listed in Table 2 for both simulations (Sim.) and experimental (Exp.).

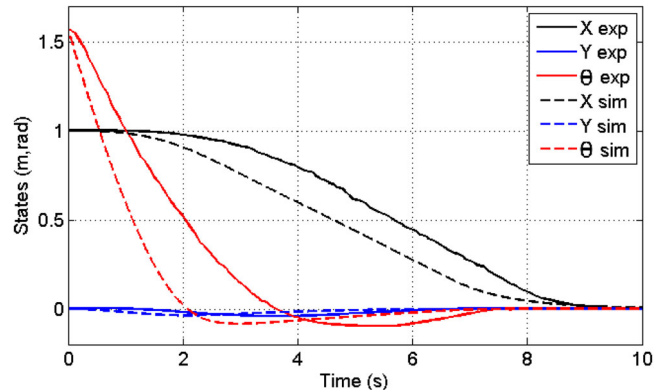
To quantify the regulation process, we introduce a term  $\Sigma = |\tilde{q}|$ , where  $\Sigma = \sqrt{\tilde{X}^2 + \tilde{Y}^2 + \tilde{\theta}^2}$  is used to characterize the results.

Term  $\Sigma$  is introduced to measure the capabilities of the control system to vanish the error state vector, the value of term  $\Sigma$  reflects the length of the error state vector. As the value of  $\Sigma$  at steady state is smaller, this means that the SSMR reaches the target and the error state vector is vanished.

It is clear that the proposed controller could experimentally steer the SSMR to the desired point with acceptable steady state error where  $\Sigma_{ss}^{\text{exp}} \leq 0.0098$  as shown in Table 3.

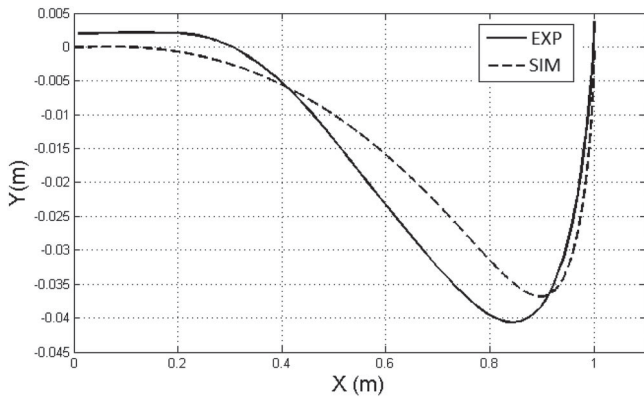
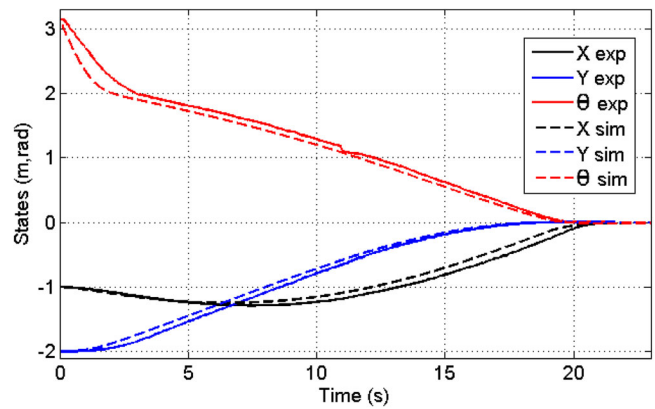
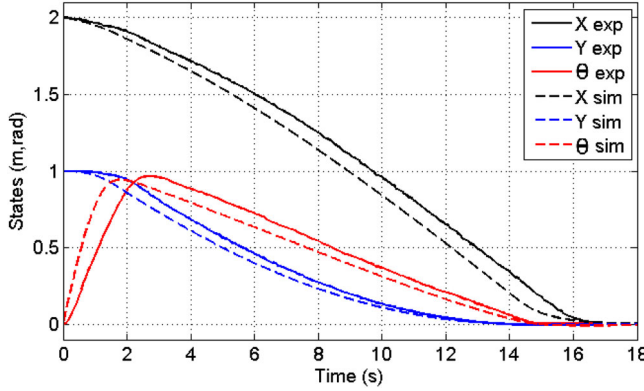
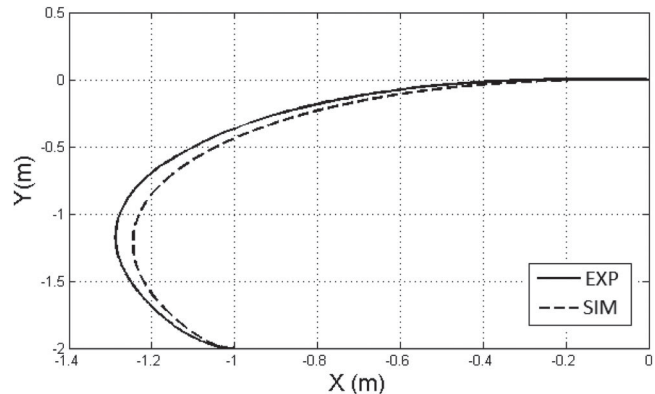
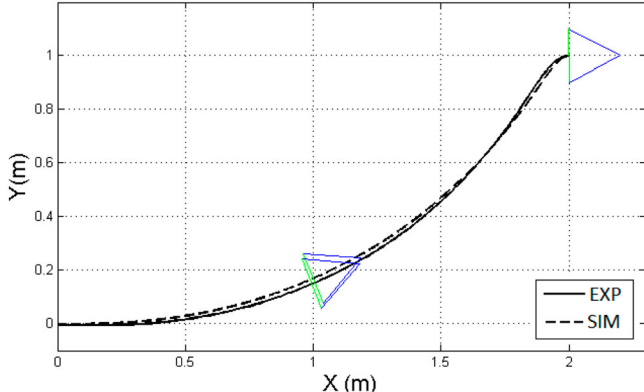
The time responses and the phase planes ( $X$  -  $Y$ ) for these cases are found in Figures 8–17, both simulation and experimental results are plotted together.

We introduce a term  $\tau$  to represent the time elapsed by the closed-loop system to steer from the initial condition to 0.03 of the initial condition, where  $\tau = t(\Sigma = 0.03 \Sigma_i)$ . Term  $\tau$  is introduced as a measure of the time consumed to vanish the error state vector, also it is used to



**Figure 12.** Time response of states  $X(m)$ ,  $Y(m)$ ,  $\theta(\text{rad})$  of SSMR Case (3).

calculate the time delay between simulations and experiments. The values of  $\tau$  for all the cases are listed in Table 4, it is observed that the experimental closed-loop system shows a delay between 0.309:0.67 (s) as shown in Figures 8, 10, 12, 14 and 16. This delay is due to the time consumed in calculation processes and communication between system components.

**Figure 13.** The  $X$ - $Y$  diagram for Case(3).**Figure 16.** Time response of states  $X$ (m),  $Y$ (m),  $\theta$ (rad) of SSMR Case (5).**Figure 14.** Time response of states  $X$ (m),  $Y$ (m),  $\theta$ (rad) of SSMR Case (4).**Figure 17.** The  $X$ - $Y$  diagram for Case(5).**Figure 15.** The  $X$ - $Y$  diagram for Case(4).

To evaluate the path in experiments with respect to simulation, the maximum drift ( $Drift_{max}$ ) is calculated for each case. The maximum drift is the maximum normal distance between the simulated and experimental paths shown in Figures 9, 11, 13, 15 and 17. The values of maximum drifts are listed in Table 4, and it varies from 0.0039 to 0.0584 (m).

### 5.3. Path following results

Secondly, the proposed path following algorithm in Section 4 is applied using the above-mentioned control law ((16), (17)) and is tested by three different trajectories. The tracking error tolerance ( $\epsilon$ ) is set to 0.1 as a simulation parameter.

All the three trajectories are represented by a set of way-points tabulated in Table 4, and the SSMR should pass through these points in sequence.

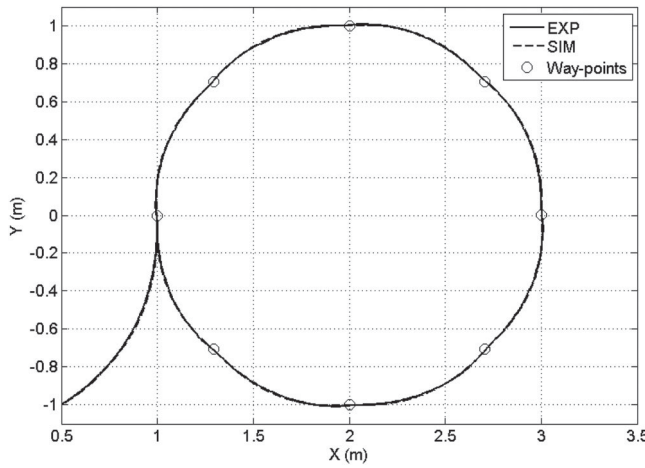
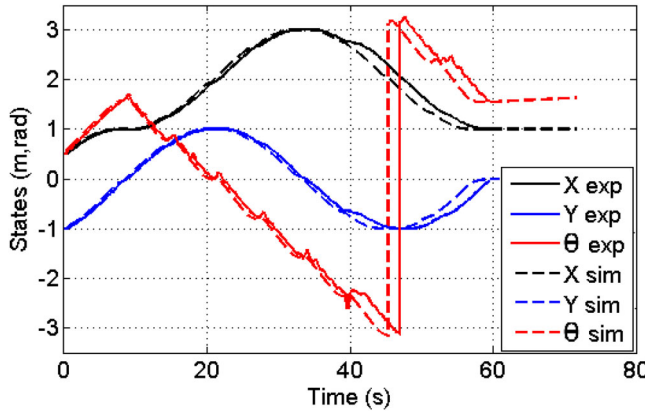
Figures 18–23 show phase plane of the SSMR for simulation, experiments and the way-points further time response of the states of the SSMR ( $X$ ,  $Y$ , and  $\theta$ ) for all the three cases.

To evaluate the proposed tracking method, we introduce the deviation ( $\gamma$ ) between achieved paths and way-points. Where, ( $\gamma$ ) is the norm of the error vector between the desired point and the nearest point in the achieved path. ( $\gamma = |\Sigma_{\text{way-point}} - \Sigma_{\text{path-nearest}}|$ ).

Figures 24 and 25 show the deviation ( $\gamma$ ) of all the cases for each way-point for simulation and experimental results respectively. The maximum deviation ( $\gamma_{max}$ )

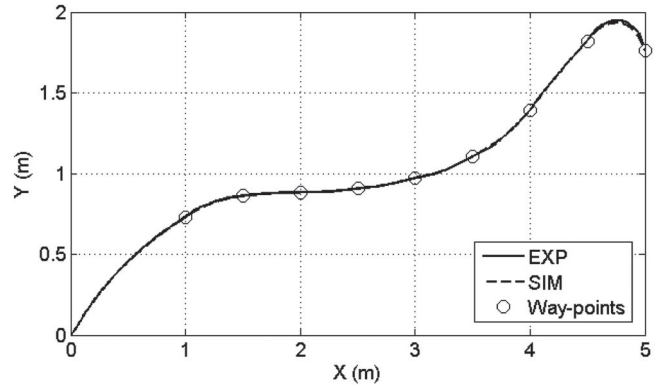
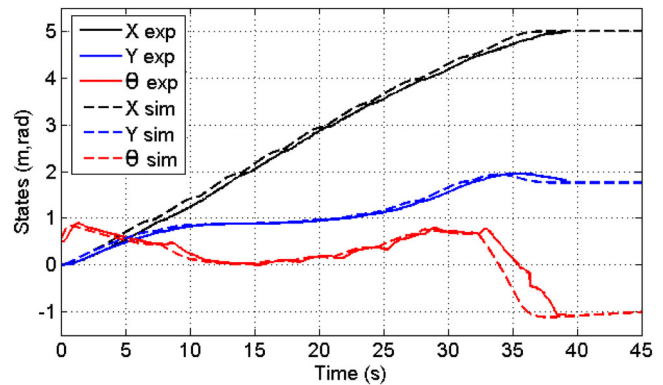
**Table 4.** Way-points on the desired trajectories for three different cases.

| Point | Case (1) |       |                | Case (2) |      |                | Case (3) |      |                |
|-------|----------|-------|----------------|----------|------|----------------|----------|------|----------------|
|       | X(m)     | Y(m)  | $\theta$ (rad) | X(m)     | Y(m) | $\theta$ (rad) | X(m)     | Y(m) | $\theta$ (rad) |
| 1     | 0.50     | -1.00 | 0.50           | 0.00     | 0.00 | 0.50           | 0.00     | 0.00 | 0.50           |
| 2     | 1.00     | 0.00  | 1.57           | 1.00     | 0.73 | 0.44           | 1.00     | 0.49 | 1.01           |
| 3     | 1.29     | 0.71  | 0.78           | 1.50     | 0.86 | 0.10           | 1.50     | 0.81 | 0.11           |
| 4     | 2.00     | 1.00  | 0.00           | 2.00     | 0.88 | 0.021          | 2.00     | 0.90 | 0.37           |
| 5     | 2.71     | 0.71  | -0.78          | 2.50     | 0.90 | 0.08           | 2.50     | 1.23 | 0.73           |
| 6     | 3.00     | 0.00  | -1.57          | 3.00     | 0.97 | 0.18           | 3.00     | 1.71 | 0.74           |
| 7     | 2.71     | -0.71 | -2.35          | 3.50     | 1.11 | 0.36           | 3.50     | 2.06 | 0.36           |
| 8     | 2.00     | -1.00 | -3.14          | 4.00     | 1.39 | 0.65           | 4.00     | 2.05 | -0.40          |
| 9     | 1.29     | -0.71 | 2.35           | 4.50     | 1.82 | 0.66           | 4.50     | 1.67 | -0.80          |
| 10    | 1.00     | 0.00  | 1.57           | 5.00     | 1.75 | -1.06          | 5.00     | 1.13 | -0.78          |
| 11    |          |       |                |          |      |                | 5.50     | 0.81 | -0.15          |
| 12    |          |       |                |          |      |                | 6.00     | 1.07 | 0.87           |
| 13    |          |       |                |          |      |                | 6.50     | 1.93 | 1.11           |
| 14    |          |       |                |          |      |                | 7.00     | 2.70 | 0.40           |

**Figure 18.** Phase plane of both simulation, experimental results and way-points for tracking Case (1).**Figure 19.** Time response of states  $X(m)$ ,  $Y(m)$ ,  $\theta(\text{rad})$  of SSMR for tracking Case (1).

for both numerical simulation and real experiments are tabulated in Table 5.

It is clear that the proposed control system which is illustrated in Figure 3 achieve good tracking performance

**Figure 20.** Phase plane of both simulation, experimental results and way-points for tracking Case (2).**Figure 21.** Time response of states  $X(m)$ ,  $Y(m)$ ,  $\theta(\text{rad})$  of SSMR for tracking Case (2).

with maximum deviation shown in Table 5. It worth to mention that the path between way-points is generated by the control law governed by Equations ((15), (16)), while we can change both shape and curvature of this path by selection of the relative value of  $k_1/k_2$  taking into consideration the criteria discussed in Section 4.2.

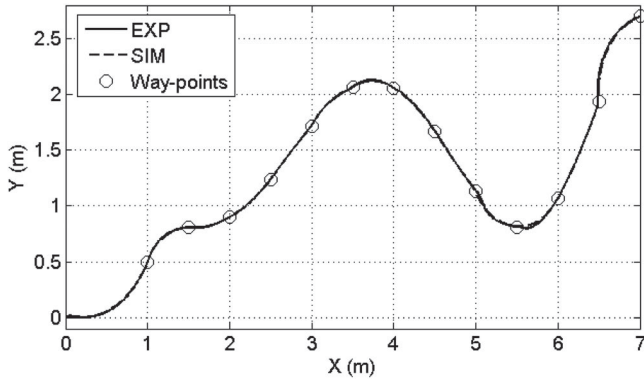


**Figure 22.** Phase plane of both simulation, experimental results and way-points for tracking Case (3).

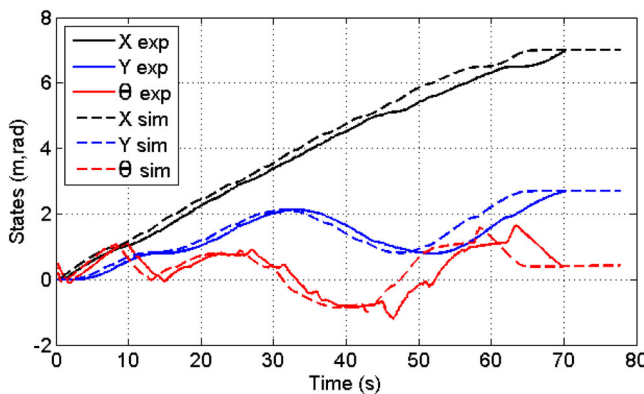


**Figure 23.** Time response of states  $X(m)$ ,  $Y(m)$ ,  $\theta(\text{rad})$  of SSMR for tracking Case (3).

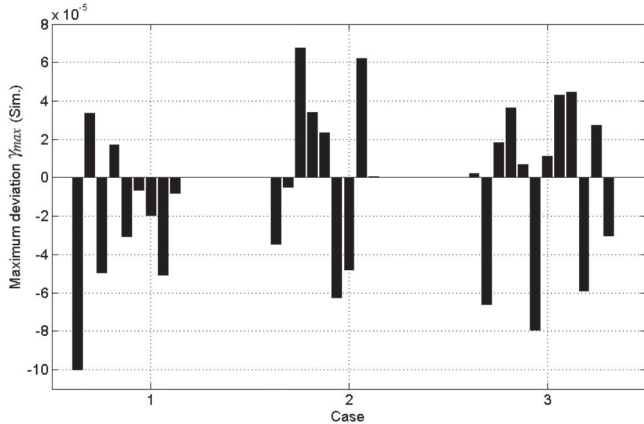


**Figure 24.** Deviation  $\gamma$  of all the cases for each way-point for simulation results.

## 6. Conclusion

A state feedback control law is designed to stabilize the SSMR, which is described by the underactuated driftless nonlinear dynamics associated with nonholonomic constraints. A discontinuous state transformation is introduced by means of signed polar transformation, thus

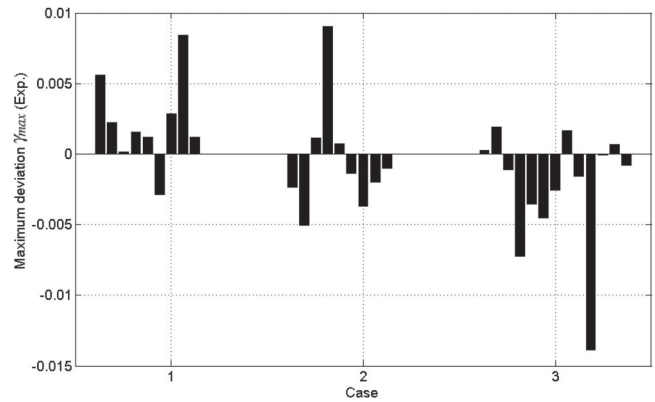


**Figure 25.** Deviation  $\gamma$  of all the cases for each way-point for experimental results.

**Table 5.** The values of  $\gamma_{\max}$  for the three cases of trajectory tracking.

|              | Case            | 1                     | 2                     | 3                     |
|--------------|-----------------|-----------------------|-----------------------|-----------------------|
| Simulation   | $\gamma_{\max}$ | $9.97 \times 10^{-5}$ | $6.76 \times 10^{-5}$ | $7.93 \times 10^{-5}$ |
| Experimental | $\gamma_{\max}$ | $8.4 \times 10^{-3}$  | $9 \times 10^{-3}$    | $13.9 \times 10^{-3}$ |

the system became in a suitable form to design a regulation control law. We consider the kinematics of the SSMR and the influence of ICR shift from COG. Exponential stabilization of the closed-loop control system is proved, except for certain initial conditions. A point-to-point tracking algorithm is proposed to be merged with the posture controller, this method enables a model-based controller to be used in a realistic manner. An adaptive gain selection criterion is introduced to consider the actuators capacity during real implementation. The closed-loop system is simulated using MATLAB environment, and results show asymptotic stability for point stabilization and good tracking capabilities. The proposed control system is validated experimentally on a reconfigured TURTLEBOT3 Burger. The experimental results are analyzed by different aspects, steady state error, delay time, maximum drift and maximum deviation. These analyses show that the proposed controller succeeded to steer the SSMR to the desired point without shutting with moderate delay and mild path drift. Experiments also showed the effectiveness of the tracking algorithm, where the SSMR succeeded to cross over all the way-points. The proposed control system enables for more realistic path tracking during demining or hazard exploration in unprepared terrains.

## Disclosure statement

No potential conflict of interest was reported by the authors.

## Funding

The first author is fully funded from the Cultural Affairs and Missions Department, Egyptian Ministry of Higher Education (MoHE), thus he would like to express his gratitude to the funder for securing this grant.

## Notes on contributors

**Fady Ibrahim** is an assistant professor in the Department of Automotive Engineering, Ain Shams University, Cairo, Egypt. He received the BSc and MSc degrees in mechanical engineering and automotive section from Ain Shams University, Cairo, Egypt, in 2006 and 2013, respectively. In 2018, he obtained his PhD degree in mechatronics and robotics engineering from Egypt-Japan University of Science and Technology, Alexandria, Egypt. He was a research assistant in Ain Shams University from 2008 to 2014. From October 2017 to May 2018 he became a research fellow at Waseda University, Tokyo, Japan. His current research interests include control of wheeled mobile robots, trajectory planning and tracking in unstructured environment and automotive powertrain control and hybrid cars and Autonomous vehicles.

**A. A. Abouelsoud** is a Professor of Automatic Control at the Electronics and Communications Engineering Department, Cairo University. He received his BSc in Electronics and Communications Engineering in 1986 (distinction with honor), MSc in Control Engineering in 1989, and PhD in Control Engineering in 1995, all from Cairo University, Egypt. He was a Visiting Assistant Professor at Washington State University, USA in 2001. Prof Abouelsoud joined Sultan Qaboos University, Oman in 2008 to 2009, and Taibah University, KSA in 2011 to 2012. He joined Egypt-Japan University of Science and Technology, E-JUST, since 2013 to 2018. He works as a part-time external moderator of Jomo Kenyatta University for agriculture and technology, Kenya, for the undergraduate and postgraduate programs of Mechatronics Engineering. Prof Abouelsoud has published more than 40 journal and 30 conference papers in automatic control, and robotics. His research interests are in nonlinear and adaptive control, process control and distributed control systems.

**Ahmed M. R. Fath Elbab** was born in Cairo, Egypt, in 1974. He received the MSc and PhD degrees from Assiut University, Assiut, Egypt, in 2002 and 2008, respectively. His PhD work was in the field of micromachined tactile sensors for robotics and medical applications. From October 2006 to October 2008, he was a Visiting Researcher at the Tabata Laboratory, Kyoto University, Kyoto, Japan. During this period, he gained experience in microfabrication experimentally. Since January 2009, he has been a Lecturer (Assistant Professor) in the Department of Mechanical Engineering, Faculty of Engineering, Assiut University, and then became Associate Professor in December 2014. Currently, he is the Department head of the Mechatronics and Robotics Engineering Department, Egypt-Japan University of Science and Technology, Alexandria, Egypt. His current interests include microsensors (principle, simulation, design, and fabrication), micromachining and its application in MEMS, tactile sensing systems (tactile sensing and display), micro energy harvesting devices, and microfluidics systems. Dr Fath El Bab was a recipient of the Best Ph.D. Thesis Prize in Engineering Sciences from Assiut University in 2010.

**Tetsuya Ogata** received the BS, MS, and DE degrees in mechanical engineering from Waseda University, Japan, in 1993, 1995, and 2000, respectively. He was a Research Associate with Waseda University from 1999 to 2001. From 2001 to 2003, he was a Research Scientist with the RIKEN Brain Science Institute. From 2003 to 2012, he was an Associate Professor with the Graduate School of Informatics, Kyoto University. Since 2012, he has been a Professor with the Faculty of Science and Engineering, Waseda University. From 2009 to 2015, he was a JST (Japan Science and Technology Agency) PREST Researcher. He is currently a Joint Appointed Fellow with the Artificial Intelligence Research Center, National Institute of Advanced Industrial Science and Technology. His current research interests include human–robot interaction, dynamics of human–robot mutual adaptation, and inter-sensory translation in robot systems with neuro-dynamical models.

## References

- [1] Wong JY. Theory of ground vehicles. New York: Wiley; 2001.
- [2] Brockett RW. Asymptotic stability and feedback stabilization. In: Brockett R, Millman RS, Sussmann HJ, editors. Differential geometric control theory. Vol. 27(1). Boston: Birkhäuser; 1983. p. 181–191.
- [3] Dong JF, Sebastian SE, Lim TM, et al. Autonomous indoor vehicles. In: Handbook of manufacturing engineering and technology. Springer; 2015. p. 2301–2346.
- [4] Urakubo T, Tsuchiya K, Tsujita K. Motion control of a two-wheeled mobile robot. *Adv Robot.* 2001;15(7):711–728.
- [5] Blažič S. A novel trajectory-tracking control law for wheeled mobile robots. *Robot Auton Syst.* 2011;59(11):1001–1007.
- [6] Wang T-Y, Tsai C-C, Pang J-L. Nonlinear regulation and path tracking of a wheeled mobile robot in polar coordinates. *J Chin Inst Eng.* 2005;28(6):925–933.
- [7] Tayebi A, Rachid A. Adaptive controller for non-holonomic mobile robots with matched uncertainties. *Adv Robot.* 2000;14(2):105–118.
- [8] Urakubo T. Discontinuous feedback stabilization of a class of nonholonomic systems based on Lyapunov control. In: Proceedings of the Fifth International Workshop on Robot Motion and Control; 2005; RoMoCo'05. IEEE; 2005. p. 91–96.
- [9] Yoon D-Y, Oh S-R, Park G-T. An effective posture stabilizer for differential drive mobile robots. *Adv Robot.* 2003;17(9):951–965.
- [10] Ibrahim F, Abouelsoud A, Elbab AMF. Time-varying fuzzy logic controller of skid-steering mobile robot based on Lyapunov stability. In: 23rd International Conference on Mechatronics and Machine Vision in Practice (M2VIP); 2016. IEEE; 2016. p. 1–6.
- [11] Ke-Cai C. Global  $\kappa$ -exponential tracking control of non-holonomic systems in chained-form by output feedback. *Acta Automat Sinica.* 2009;35(5):568–576.
- [12] JIANGdagger Z-P, Nijmeijer H. Tracking control of mobile robots: a case study in backstepping. *Automatica.* 1997;33(7):1393–1399.
- [13] Resende CZ, Carelli R, Sarcinelli-Filho M. A nonlinear trajectory tracking controller for mobile robots with velocity limitation via fuzzy gains. *Control Eng Pract.* 2013;21(10):1302–1309.

- [14] Pears NE. *Mobile robot tracking of pre-planned paths*. *Adv Robot*. 2001;15(1):97–107.
- [15] Wada N, Tagami S, Saeki M. *Path-following control of a mobile robot in the presence of actuator constraints*. *Adv Robot*. 2007;21(5–6):645–659.
- [16] Keighobadi J, Sadeghi MS, Fazeli KA. *Dynamic sliding mode controller for trajectory tracking of nonholonomic mobile robots*. *IFAC Proc Vol*. 2011;44(1):962–967.
- [17] Salgado I, Cruz-Ortiz D, Camacho O, et al. *Output feedback control of a skid-steered mobile robot based on the super-twisting algorithm*. *Control Eng Pract*. 2017;58:193–203.
- [18] Martins NA, De Pieri ER, Moreno UF, et al. *Pd-super-twisting second order sliding mode tracking control for a nonholonomic wheeled mobile robot*. *IFAC Proc Vol*. 2014;47(3):3827–3832.
- [19] Matraji I, Al-Durra A, Haryono A, et al. *Trajectory tracking control of skid-steered mobile robot based on adaptive second order sliding mode control*. *Control Eng Pract*. 2018;72:167–176.
- [20] Merabti H, Belarbi K, Bouchemal B. *Nonlinear predictive control of a mobile robot: a solution using metaheuristics*. *J Chin Inst Eng*. 2016;39(3):282–290.
- [21] Kim T, Kim W, Choi S, et al. *Path tracking for a skid-steer vehicle using model predictive control with on-line sparse gaussian process*. *IFAC-PapersOnLine*. 2017;50(1):5755–5760.
- [22] Škrjanc I, Klančar G. *A comparison of continuous and discrete tracking-error model-based predictive control for mobile robots*. *Robot Auton Syst*. 2017;87:177–187.
- [23] Ye J. *Tracking control of two-wheel driven mobile robot using compound sine function neural networks*. *Connect Sci*. 2013;25(2–3):139–150.
- [24] Ye J. *Tracking control of a non-holonomic wheeled mobile robot using improved compound cosine function neural networks*. *Inter J Control*. 2015;88(2):364–373.
- [25] Li S, Ding L, Gao H, et al. *Adaptive neural network tracking control-based reinforcement learning for wheeled mobile robots with skidding and slipping*. *Neurocomputing*. 2018;283:20–30.
- [26] Ahmed SA, Petrov MG. *Trajectory control of mobile robots using type-2 fuzzy-neural PID controller*. *IFAC-PapersOnLine*. 2015;48(24):138–143.
- [27] Huang J, Wen C, Wang W, et al. *Adaptive output feedback tracking control of a nonholonomic mobile robot*. *Automatica*. 2014;50(3):821–831.
- [28] Gonzalez R, Fiacchini M, Alamo T, et al. *Adaptive control for a mobile robot under slip conditions using an LMI-based approach*. *Eur J Control*. 2010;16(2):144–155.
- [29] Martins FN, Celeste WC, Carelli R, et al. *An adaptive dynamic controller for autonomous mobile robot trajectory tracking*. *Control Eng Pract*. 2008;16(11):1354–1363.
- [30] Huang D, Zhai J, Ai W, et al. *Disturbance observer-based robust control for trajectory tracking of wheeled mobile robots*. *Neurocomputing*. 2016;198:74–79.
- [31] Cui M, Liu W, Liu H, et al. *Unscented Kalman filter-based adaptive tracking control for wheeled mobile robots in the presence of wheel slipping*. In: 2016 12th World Congress on Intelligent Control and Automation (WCICA). IEEE; 2016. p. 3335–3340.
- [32] Hu C, Jing H, Wang R, et al. *Robust  $H^\infty$  output-feedback control for path following of autonomous ground vehicles*. *Mech Syst Signal Proc*. 2016;70:414–427.
- [33] Han KL, Lee JS. *Iterative path tracking of an omnidirectional mobile robot*. *Adv Robot*. 2011;25(13–14):1817–1838.
- [34] Yang H, Fan X, Xia Y, et al. *Robust tracking control for wheeled mobile robot based on extended state observer*. *Adv Robot*. 2016;30(1):68–78.
- [35] Avendaño-Juárez JL, Hernández-Guzmán VM, Silva-Ortigoza R. *Velocity and current inner loops in a wheeled mobile robot*. *Adv Robot*. 2010;24(8–9):1385–1404.
- [36] Shi S, Yu X, Khoo S. *Robust finite-time tracking control of nonholonomic mobile robots without velocity measurements*. *Int J Control*. 2016;89(2):411–423.
- [37] Begnini M, Bertol DW, Martins NA. *A robust adaptive fuzzy variable structure tracking control for the wheeled mobile robot: simulation and experimental results*. *Control Eng Pract*. 2017;64:27–43.
- [38] Xin L, Wang Q, She J, et al. *Robust adaptive tracking control of wheeled mobile robot*. *Robot Auton Syst*. 2016;78:36–48.
- [39] Nazari V, Naraghi M. *Sliding mode fuzzy control of a skid steer mobile robot for path following*. In: 10th International Conference on Control, Automation, Robotics and Vision. ICARCV; 2008. IEEE; 2008. pp. 549–554.
- [40] Campa MG, Gordillo JL, Soto R. *Speed and point-to-point control for trajectory tracking of a skid-steered mobile robot*. In: 11th IEEE International Conference on Control & Automation (ICCA). IEEE; 2014. p. 637–642.
- [41] Lepej P, Maurer J, Uran S, et al. *Dynamic arc fitting path follower for skid-steered mobile robots*. *Int J Adv Robot Syst*. 2015;12(10):139.
- [42] Moustris GP, Tzafestas SG. *Switching fuzzy tracking control for mobile robots under curvature constraints*. *Control Eng Pract*. 2011;19(1):45–53.
- [43] Hernández-Guzmán VM, Silva-Ortigoza R, Márquez-Sánchez C. *A pd path-tracking controller plus inner velocity loops for a wheeled mobile robot*. *Adv Robot*. 2015;29(16):1015–1029.
- [44] Sordalen O, De Wit CC. *Exponential control law for a mobile robot: extension to path following*. *IEEE Trans Robot Autom*. 1993;9(6):837–842.
- [45] Kozłowski K, Pazderski D. *Modeling and control of a 4-wheel skid-steering mobile robot*. *Int J Appl Math Comput Sci*. 2004;14:477–496.
- [46] Jun J-Y, Hua M-D, Benamar F. *A trajectory tracking control design for a skid-steering mobile robot by adapting its desired instantaneous center of rotation*. In: 2014 IEEE 53rd Annual Conference on Decision and Control (CDC). IEEE; 2014. p. 4554–4559.
- [47] Tayebi A, Rachid A. *A unified discontinuous state feedback controller for the path-following and the point-stabilization problems of a unicycle-like mobile robot*. In: Proceedings of the 1997 IEEE International Conference on Control Applications. IEEE; 1997. p. 31–35.
- [48] Coron J-M. *Global asymptotic stabilization for controllable systems without drift*. *Math Control Signal Syst*. 1992;5(3):295–312.
- [49] Samson C. *Time-varying feedback stabilization of car-like wheeled mobile robots*. *Int J Robot Res*. 1993;12(1):55–64.
- [50] Samson C. *Control of chained systems application to path following and time-varying point-stabilization of mobile robots*. *IEEE Trans Auto Control*. 1995;40(1):64–77.

- [51] Tayebi A, Tadjine M, Rachid A. Path-following and point-stabilization control laws for a wheeled mobile robot. In: UKACC International Conference on Control'96 (Conf. Publ. No. 427). Vol. 2. IET; 1996, p. 878–883.
- [52] Chen C-Y, Li T-HS, Yeh Y-C, et al. *Design and implementation of an adaptive sliding-mode dynamic controller for wheeled mobile robots*. Mechatronics. 2009;19(2):156–166.
- [53] Yang J-M, Kim J-H. *Sliding mode control for trajectory tracking of nonholonomic wheeled mobile robots*. Robot Auto IEEE Trans. 1999;15(3):578–587.
- [54] Martins NA, Elyousseff ES, Bertol DW, et al. *Trajectory tracking of a nonholonomic mobile robot with kinematic disturbances: a variable structure control design*. Latin Amer Trans IEEE (Revista IEEE Amer Latina). 2011;9(3):276–283.
- [55] Morin P, Samson C. *Control of nonholonomic mobile robots based on the transverse function approach*. Robot IEEE Trans. 2009;25(5):1058–1073.
- [56] Li X, Wang Z, Chen X, et al. Adaptive control of unicycle-type mobile robots with longitudinal slippage. In: American Control Conference (ACC). IEEE; 2016. p. 1637–1642.
- [57] Astolfi A. *Discontinuous control of nonholonomic systems*. Syst Control Lett. 1996;27(1):37–45.
- [58] Ibrahim F, Abouelsoud A, Fath El Bab AM, et al. *Discontinuous stabilizing control of skid-steering mobile robot (SSMR)*. J Int Robot Sys. 20181–14.
- [59] Astolfi A. *Exponential stabilization of a wheeled mobile robot via discontinuous control*. J Dynam Syst Meas Control. 1999;121:121–125. Transactions-American Society Of Mechanical Engineers.
- [60] Fontes F, Magni L, et al. *Min-max model predictive control of nonlinear systems using discontinuous feedbacks*. IEEE Trans Automat Control. 2003;48(10):1750–1755.
- [61] Duong SC, Kinjo H, Uezato E, et al. A discontinuous control of a nonholonomic wheeled mobile robot. In: ICCAS-SICE. IEEE; 2009, p. 2464–2467.
- [62] Turtlebot3 burger; 2018. Available from: <http://www.robotis.us/turtlebot-3/>.
- [63] Opencr1 control board; 2018. Available from: <http://emanual.robotis.com/docs/en/parts/controller/opencr10/>.
- [64] AMS contact-less absolute wheel encoder; 2018. Available from: <https://ams.com/as5601>.